DOI: 10.1002/aelm.201900975
Article type: (**Full Paper**)

Intrinsic Dipole Coupling in Two–Dimensional van der Waals Ferroelectrics for Gate-Controlled Switchable Rectifier

*Mingjin Dai, Kai Li, Fakun Wang, Yunxia Hu, Jia Zhang, Tianyou Zhai, Bin Yang, Yongqing Fu, Wenwu Cao, Dechang Jia, Yu Zhou, PingAn Hu**

M. Dai, Y. Hu, Prof. D. Jia, Y. Zhou, P. Hu
School of Materials Science and Engineering
MOE Key Laboratory of Micro-Systems and Micro-Structures Manufacturing
Harbin Institute of Technology
Harbin 150001, China
E-mail: hupa@hit.edu.cn
K. Li, Prof. B. Yang, W. Cao
Condensed Matter Science and Technology Institute
School of Instrument Science and Engineering
Harbin Institute of Technology
Harbin 150001, China
F. Wang, Prof. T. Zhai
State Key Laboratory of Material Processing and Die and Mould Technology
School of Materials Science and Engineering
Huazhong University of Science and Technology
Wuhan 430074, China
Prof. Y. Fong
Department of Mathematics and Materials Research Institute
The Pennsylvania State University
University Park, Pennsylvania 16802, USA
Prof. D. Jia, Y. Zhou, P. Hu
Key Laboratory of Advanced Structural-Functional Integration Materials & Green Manufacturing Technology
Harbin Institute of Technology
Harbin 150080, China

Abstract: Miniaturization of device elements, such as ferroelectric diodes, depends on the downscaling of the ferroelectric film, which is also crucial for developing high-density information storage technologies of ferroelectric random access memories (FeRAMs). Recently emerged ferroelectric two-dimensional (2D) van der Waals (vdWs) layered materials bring an additional opportunity for further increase the density of FeRAMs. Herein, we have designed and fabricated lateral switchable rectifier based on atomically thin 2D α-In_2Se_3 ferroelectric diodes, which breaks the thickness limitation of conventional ferroelectric films and achieved an unprecedented level of miniaturization. This is realized through the interrelated coupling between out-of-plane and in-plane dipoles at room temperature, i.e., horizontal polarization reversal can be effectively controlled through a vertical electric field. Being further explored as a switchable rectifier, the obtained maximum value of rectification ratio for the α-In_2Se_3 based ferroelectric diode can reach up to 2.5×10^3. These results indicate that our 2D ferroelectric semiconductors can offer a pathway to develop next-generation multifunctional electronics.

Keywords: two-dimensional materials, ferroelectric, gate-tunable, asymmetric contact, dipole coupling

1. Introduction

Ferroelectric random access memories (FeRAMs), in which the data are encoded through reversible polarization in ferroelectric films, are a growing number of alternative non-volatile random-access memory technologies with fast write speed, large read/write cycle endurance and low power consumption.[1-4] The vdW 2D ferroelectrics have no physical limit of critical thickness, which has been the main issue in conventional ferroelectric films.[5-7] Thus the out-of-plane (OOP) and in-plane (IP) ferroelectricity could be easily achieved in some atomically thin vdW 2D ferroelectric films, such as SnTe, $CuInP_2S_6$, $LiAlTe_2$, and In_2Se_3.[8-14] Particularly, different from ultrathin SnTe and $CuInP_2S_6$, whose polarization only involves either pure IP or OOP orientations, atomically thin 2D In_2Se_3 shows both IP and OOP ferroelectricity in its ground state of the α phase.[12] And the IP and OOP polarizations of 2D α-In_2Se_3 have strong interrelated couping.[15-18] In previous work, we found that the OOP dipole in trilayer In_2Se_3 is locked by the IP lattice asymmetry and its switching is related to the inversion of IP lattice orientation.[18] Up to date, there are few reports in the literature regarding ultimate miniature switchable rectifiers made of these atomically thin 2D ferroelectrics by utilizing the dipole polarization coupling.[19]

Here, we report the fabrication of a gate-controlled switchable ferroelectric diode based on the single crystal of α-In_2Se_3 by utilizing the interrelated coupling effect of OOP and IP polarizations (**Figure 1**). This ferroelectric diode can be inversed effectively by switching the gate bias between the negative (Figure 1a) and the positive configurations (Figure 1b). With a good rectification property of the ferroelectric diode, a switchable dynamic half-wave rectifier was realized. This kind of 2D ferroelectric diode has the advantages of simplicity in fabrication compatibility with complementary metal-oxide-semiconductor (CMOS) technology, and superior electrical rectifying characteristics, showing great potential for future integrated electronic applications.

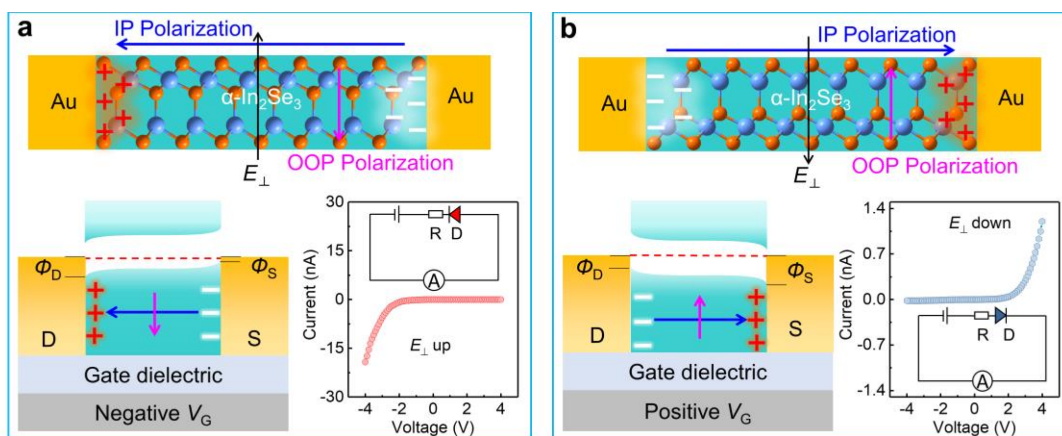

Figure 1. The switchable ferroelectric diode based on 2D α-In_2Se_3 single crystal. a) Top: Schematic diagram of the α-In_2Se_3 device with downward IP and leftward OOP polarization configurations. Left bottom: Band diagrams under corresponding polarization configurations. Right bottom: A typical *I-V* curves of In_2Se_3 device with corresponding configurations. Inset: the equivalent circuit diagram. b) Top: Schematic diagram of the α-In_2Se_3 device with opposite IP and OOP polarization configurations. Left bottom: Band diagrams under corresponding polarization configurations. Right bottom: A typical *I-V* curves of In_2Se_3 device with corresponding configurations. Inset: the equivalent circuit diagram.

2. Results and Discussion

2.1. Synthesis and structural characterization

The atomically thin α-In_2Se_3 single crystals were synthesized by using chemical vapor deposition (CVD) method (see Methods and Figure S1, Supporting Information). And its structure was characterized by Raman and transition electron microscopy (Figure. S2 and S3, Supporting Information). The α-In_2Se_3 exhibits an *R3m* space group without an inversion center, and there are three monolayers in a unit cell, which consists of five covalently bonded Se/In atomic planes as shown in **Figure 2**a. Owing to its non-centrosymmetric crystal structure, it processes spontaneous IP and OOP polarizations, which are denoted by blue and pink arrows, respectively. In addition, second harmonic generation (SHG) measurements were used to investigate the broken symmetry in the α-In_2Se_3 nanoflake.[20,21] The SHG intensity mapping was firstly carried out on a triangle α-In_2Se_3 single crystal and the result is shown in Figure 2b. The homogenous SHG intensity reveals the high uniformity of crystal structures for the CVD grown α-In_2Se_3 nanoflakes. Furthermore, the corresponding angle dependent polarized SHG intensities were obtained to investigate the crystal

symmetry. The SHG measurements were carried out by rotating the sample with a fixed polarization which is parallel to the incident laser (Figure 2c). A six-fold symmetry observed from the SHG pattern demonstrates a three-fold rotational symmetry of *R3m* space group for the α-In_2Se_3.[14]

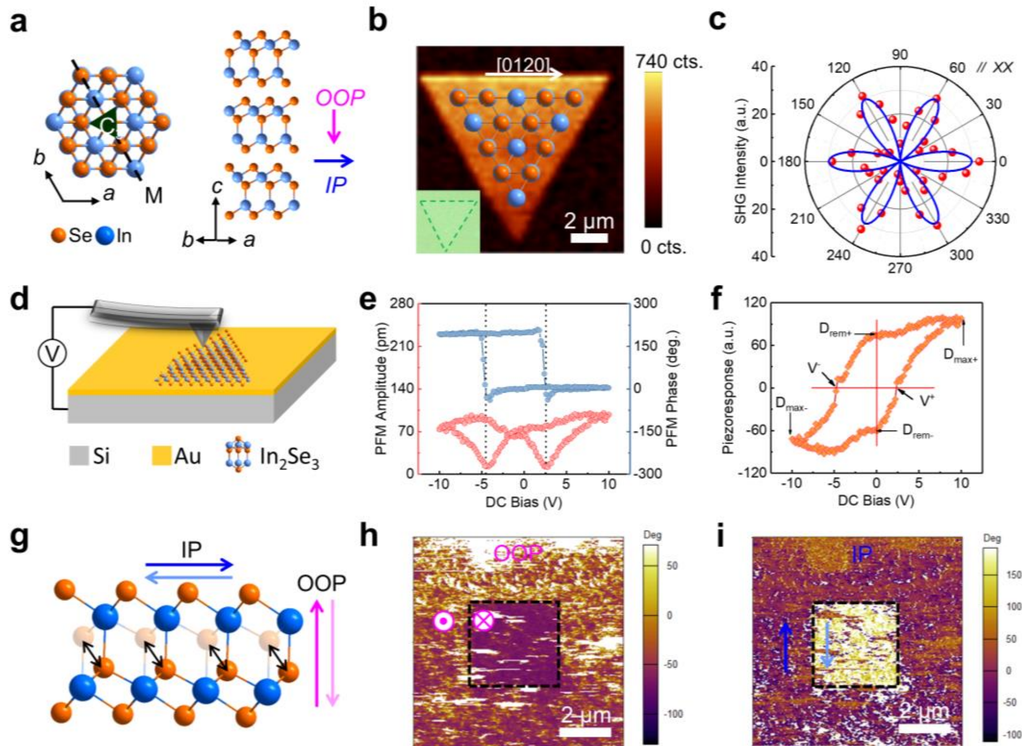

Figure 2. Ferroelectricity and polarization coupling in α-In_2Se_3 single crystal. a) The crystal structure of α-In_2Se_3 belonging to *R3m* space group. b) SHG intensity mapping of a triangle α-In_2Se_3 nanoflake on a mica substrate. Inset: the corresponding optical image of the same sample. c) The polarized SHG intensity pattern of a triangle α-In_2Se_3 nanoflake on mica substrate with parallel (*XX*) to the incident laser polarization. d) PFM measurement setup for α-In_2Se_3 transferred onto Au/Si substrate. e) Off-field PFM amplitude (*A*) and phase (*φ*) hysteresis loops on the α-In_2Se_3 sample. f) The calculated piezoresponse (PR) loops for α-In_2Se_3 single crystal using PR=$A\times\cos(\varphi)$. g) The schematic model of switching coupling between OOP and IP. h) OOP PFM phase image and the corresponding. i) IP phase image of an 8 nm α-In_2Se_3 nanoflake after writing a square pattern by applying -12 V voltage.

2.2. Ferroelectricity characterizations

As shown above, the broken inversion symmetry the α phase of In_2Se_3 single crystal, which is a necessary condition for the generation of ferroelectricity, has been confirmed by Raman spectroscopy, HR-TEM, and SHG measurements. Subsequently, the direct observation of spontaneous polarization and its inversion under an external electric field was performed using the

piezoresponse force microscopy (PFM).[22] For the PFM measurements, the CVD grown In_2Se_3 nanoflake with about 5 nm thick was transferred onto a conductive substrate (e.g., heavily p-doped silicon with a 50 nm gold film) with the assistance of polymethyl methacrylate film (Figure 2d). First, the OOP spontaneous polarization switching behaviors were investigated using the high-resolution PFM (Figure S4, Supporting Information). After applying the bias field, three square ferroelectric domains were successfully obtained by opposite tip voltages (+12 V and -12 V). Two different areas are distinguishable with high contrasts in both amplitude and phase PFM images. This clearly demonstrates the existence of spontaneous polarization and its switching by an external electric field, which are the characteristics of ferroelectricity.[23.24]

The local ferroelectric loops were further investigated on the same α-In_2Se_3 nanoflake and the results are shown in Figure 2e. It displays a butterfly-like bias dependent amplitude loop and a corresponding phase hysteresis loop with a sharp change in phase up to 180°. The piezoresponse (PR) loop calculated from the amplitude (A) and phase (φ) data via the relationship of PR=$A\times\cos(\varphi)$ is shown in Figure 2f. The coercive voltages (V^- and V^+) obtained from the local piezoresponse loop measurement are approximately -4.5 and +2.6 V. The maximum piezoresponse (D_{max}) and remnant piezoresponse (D_{rem}), defined as $D_{max} = (D_{max+} - D_{max-})/2$ and $D_{rem} = (D_{rem+} - D_{rem-})/2$, are about 85 (a.u.) and 67 (a.u.), respectively.[25] Besides the CVD grown α-In_2Se_3 nanoflakes, the exfoliated α-In_2Se_3 nanosheet also exhibits ferroelectricity, which has been clearly demonstrated by the formation of ferroelectric domains (Figure S5, Supporting Information). Two distinct regions can be observed in both the amplitude and phase PFM images with ~25 pm amplitude and 180° phase difference, which clearly indicate two domains with the up and down polarization vectors. The local ferroelectric loops obtained from the same exfoliated nanosheet also reveal the ferroelectricity in α-In_2Se_3 (Figure S6, Supporting Information).

2.3. Intercorrelation of OOP and IP polarization

More importantly, the intrinsic intercorrelation of OOP and IP polarization for α-In_2Se_3 nanoflake can be clearly revealed by applying vertical PFM (V-PFM) and lateral PFM (L-PFM)

measurements.[3,15] According to previous theoretical and experimental studies, the Se atomic plane in the central layer could be vertically and laterally shifted by applying an external electric field. When the central Se atomic layer is shifted up, the OOP polarization direction will be upwards. Simultaneously, the IP polarization direction will be reversed in the lateral direction because of the IP motions of the Se atoms, thus generating its OOP motion (Figure 2g).[12,15] Here, a negative tip bias of -12 V was applied to write a square ferroelectric domain with a size of 4 μm. Afterward, the V-PFM and L-PFM analysis were performed on the same area, and the OOP and IP PFM phase images were obtained and shown in Figure 2h and 2i, respectively. The IP polarization can be reversed simultaneously, along with the OOP polarization under the external applied electric field, which provides strong evidence for the inner correlation between them. Thus, as a novel 2D ferroelectric material, the α-In_2Se_3 possesses simultaneous OOP and IP polarizations, which is totally different from other reported 2D ferroelectrics, such as SnTe and $CuInP_2S_6$. The coupling effects between OOP and IP of α-In_2Se_3 single crystal generated from its distinctly structural feature will offer more opportunities for the next-generation micro/nano electronics. The thermodynamic stability for ferroelectrics is another crucial requirement for their practical applications. To investigate the stability of α-In_2Se_3, the temperature dependent PFM measurements were carried out and the results are shown in Figure S7. With the temperature increased from 323 to 433 K, the PFM phase images, including ferroelectric domains with different polarization configurations, were recorded. When the temperature is increased to 433 K, ferroelectric domains disappear. In order to investigate the temperature dependence of ferroelectricity of the α-In_2Se_3 nanoflakes, the phase difference (ΔPhase) between two domains (labeled by points 1 and 2) as a function of temperature was recorded (see Figure S8, Supporting Information). The decrease of ΔPhase started at 363 K and decreased to zero at 433 K. This indicates that the ferroelectricity of α-In_2Se_3 shows excellent stability at room temperature.[18]

2.4. Electric field induced polarization reversion

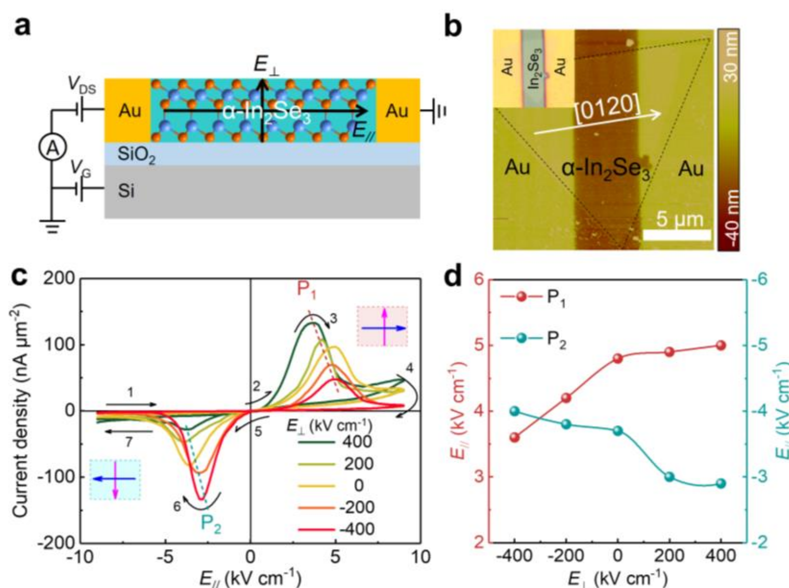

Figure 3. Reversible polarization induced electrical switching of α-In_2Se_3 devices. a) Schematic diagram of the α-In_2Se_3 device. b) AFM image of a 3.7 nm α-In_2Se_3 device. Inset: the corresponding optical device image. c) Lateral polarization inversion modulated by the vertical electric field ($E_\perp$). The arrows and numbers represent the measurement direction and sequence. d) $E_\perp$-dependent lateral current peak positions.

Figure 3a shows an α-In_2Se_3 single-crystal based device by using gold as both the source and drain electrodes. Here, the vertical electric field was applied by using a 100 nm thick SiO_2 dielectric and n-doped Si electrode. An atomic force microscope (AFM) image of the device is displayed in Figure 3b. Two Au electrodes were deposited onto the α-In_2Se_3 single crystal (triangle area), and the corresponding optical device image is shown in the inset in Figure 3b. The measured thickness of the α-In_2Se_3 single crystal is about 3.7 nm (4-layer), and the channel length is around 5 μm. Considering the anisotropy of ferroelectric polarization in the α-In_2Se_3 single crystal, the channel direction is set to along the [0120] crystal axis (as shown in Figure 2b), which is believed to be the direction of IP spontaneous polarization for the α-In_2Se_3 single crystal.[12] The *I-V* characterizations were recorded by applying different vertical electric fields (Figure 3c). All these results clearly show the existence of current peaks, indicating that the lateral IP polarization can be switched under the lateral electric field.[26] Interestingly, compared the current peaks with different vertical electric fields, the current peaks (P_2) in the third quadrant are decreased when the vertical electric field

changed from negative to positive, whereas those peaks (P_1) in the first quadrant show a totally opposite trend. At the same time, the coercive voltages in the first quadrant (P_1), which can be extracted from the current peak positions, are increased with a vertical electric field, whereas those in the second quadrant (P_2) are decreased with the vertical electric field (Figure 3d). The current peak P_1 is caused by the lateral IP polarization switching from leftward to rightward. Meanwhile, the vertical OOP polarization will be reversed from downward to upward. With the vertical electric field changed from positive (upward) to negative (downward), the inversion of vertical OOP polarization was suppressed and became difficult. Thus, the current peaks at P_1 are decreased, and the coercive voltages are increased. For the case of P_2 in the third quadrant, it exhibits the opposite trends. These results provide further evidence of the inner correlation between the IP and OOP polarization, and confirm the effective modulation of lateral IP polarization inversion by applying the vertical electric field.

2.5. Electric switching of ferroelectric diode

The ferroelectric diode exhibits a diode-like rectifying characteristics, caused by the asymmetric Schottky junction induced by the polarization, and is switchable when the related polarization is reversed.[27-30] Here, due to the interrelated IP and OOP polarizations in the 2D α-In_2Se_3 nanoflakes, we believe that the direction of a lateral ferroelectric diode based on IP polarization principle can be effectively controlled by changing the vertical electric field. Therefore, a three-terminal device, which has the same architecture as the field-effect transistor (FET) device, was designed as shown in Figure 3a. In order to investigate the diode effect induced by the vertical electric field applied from the gate bias V_G, the *I-V* curves under different gate bias were obtained and the results are shown in **Figure 4**a. It clearly shows a rectifying characteristic after applying both positive and negative gate bias V_G, whereas it shows a symmetric *I-V* curve without applying the gate bias. The currents between drain and source contacts at different gate bias were recorded and the results are shown in Figure 4b. With the value of V_G increased from -4 V to 4 V, the currents when V_{DS}= -4 V are increased, whereas currents are decreased when V_{DS}= 4V.

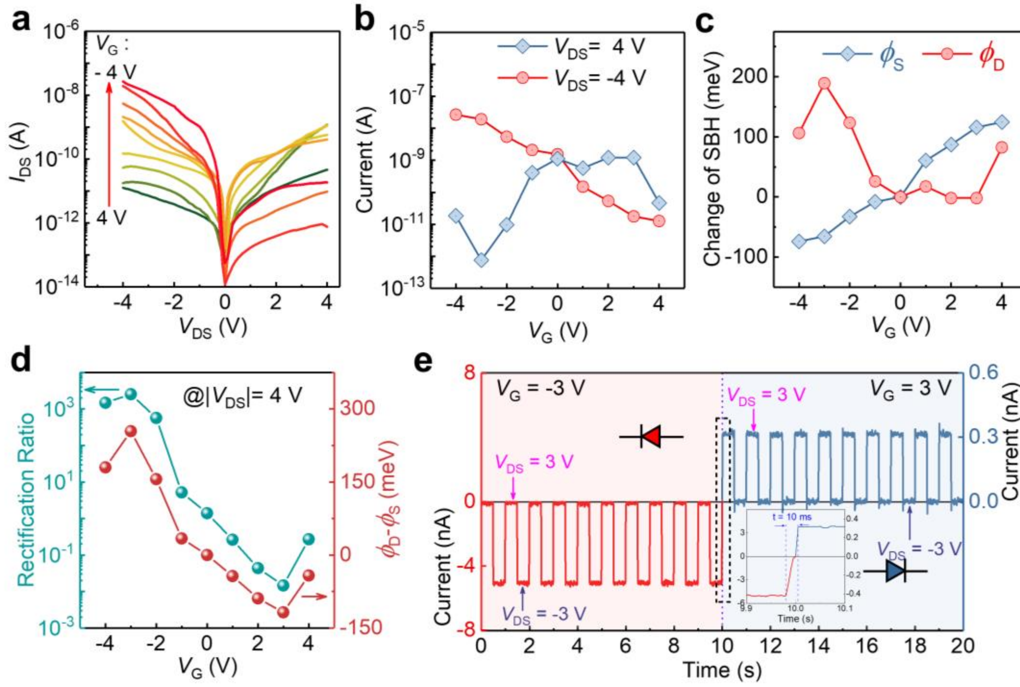

Figure 4. IP electric switching modulation by OOP electric field. a) *I*-*V* characterization of the α-In_2Se_3 device under different gate voltage. b) I_{DS} at V_{DS}= ±4 V as a function of V_G. c) The change of Schottky barrier height (SBH) at both the drain (Φ_D) and source (Φ_S) contacts as a function of V_G. d) V_G-dependent rectification ratios and difference of SBH between Φ_D and Φ_S. e) The electric switching realized by the gate voltage of -3 and +3 V. Inset: the polarization reversal time is about 10 ms.

To investigate the mechanism of current change with V_G, the change of the Schottky barrier height (SBH) $\Delta\Phi$ with V_G was obtained using the equation: $\Delta\Phi=-kT\ln(I_{VG}/I_0)$, where k is the Boltzmann constant, T is temperature, I_{VG} and I_0 are the currents with and without V_G, respectively.[31] The obtained values of $\Delta\Phi$ with the V_G are plotted in Figure 4c. For the case of V_G = 0 V, the device becomes a back-to-back Schottky diode. Owing to the same SBH at the source and drain contacts without the modulation of ferroelectric polarization, the *I*-*V* curve shows a symmetric characteristic in the first and third quadrants, and the currents at V_{DS}= -4 and 4 V are almost the same. However, for the case of a positive V_G (e.g., V_G>0), the OOP polarization changed to upward, and the IP polarization is simultaneously changed toward the source contact because of their inner correlation between OOP and IP dipoles. The SBH at the drain contact for holes is thus lower than that at the source contact, which was modulated by the local polarized charges. Therefore, the *I*-*V* curve is asymmetric and exhibits a forward diode with a significant rectification. In contrast, when the gate

bias is set to be negative (e.g., V_G<0), the OOP polarization will be changed to downward and the IP polarization will be changed toward to the drain contact. Thus, the SBH at the drain contact (Φ_D) will be increased, while that at the source contact (Φ_S) will be decreased. In this case, the device becomes a backward diode with a significant rectification, and the corresponding *I-V* curve becomes asymmetric. In fact, the applied gate bias also modulates the Fermi level in p-type α-In_2Se_3 single crystal, which is confirmed by the transfer curve of an α-In_2Se_3 based field effect transistor (Figure S10, Supporting Information). The Schottky barrier heights at both source and drain contacts will be increased (or decreased) at the same time when the gate bias is applied. As a result, the forward current for the backward diode is higher than that of the forward diode.

In addition, the rectification ratios under different gate bias and the SBH difference between drain and source contacts are plotted in Figure 4d. Two peak values of the rectification are located at V_G= -3 V and V_G= 3 V, which can reach up to 2.5×10^3 and 68, respectively. Importantly, the SBH difference shows the same characteristics and the two peaks reach up to 254.4 and -117.7 meV at the gate voltage V_G= -3 V and V_G= 3 V, respectively. This further indicates that the ferroelectric diode effect is related to the asymmetric SBH at both the drain and source contacts induced by the local polarization charges. Furthermore, the switching diode characteristics of α-In_2Se_3 based device were investigated by recording the change of current with both the V_{DS} and V_G, simultaneously (Figure 4e). With a negative V_G of -3 V, the device exhibits a backward diode, and the current can reach up to about -5 nA when V_{DS} is set to be -3 V, whereas it exhibits a forward diode when the V_G is switched to 3 V. The current is only about 0.3 nA with a V_{DS} of 3 V, which might arise from the gate induced Fermi level shift. The current switching clearly indicates that the α-In_2Se_3 ferroelectric diode shows good stability and reliability. Moreover, the polarization reversal speed can be evalued by the response time as shown in Figure 4e. The short response time (~10 ms) indicates that the ferroelectric diode exhibits a fast switching speed.

2.6. Dynamic rectifying performance

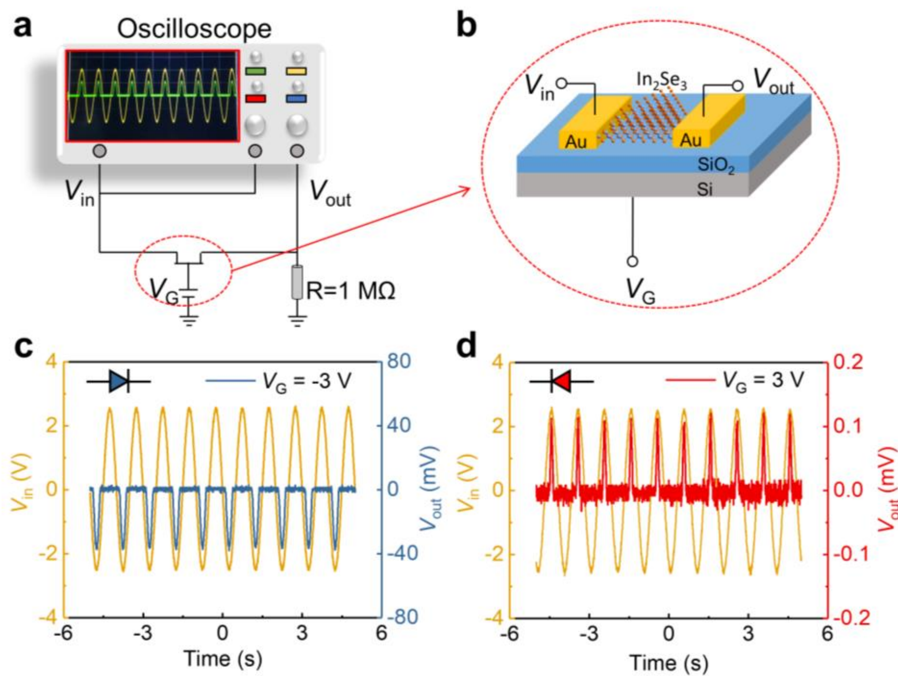

Figure 5. Dynamic rectifying performance of the α-In_2Se_3 based switchable half-wave rectifier. a) The measurement system set-up for the rectifier circuit. b) The illustration of the α-In_2Se_3 device as a rectifier. c) The input and output sine signals with forward diode configuration. d) The input and output sine signals with backward diode configuration.

Based on the large current rectification ratio of the ferroelectric diode, we further demonstrated its dynamic rectifying performance by employing it as a half-wave rectifier. The ferroelectric diode circuit scheme with the measurement system is shown in **Figure 5**a. Here, a digital oscilloscope with a preset function generator (which can as both the generator and detector), was used to apply an input alternating current (AC) voltage (sine waveform) and detect the output voltage signals of the load resistor of 1MΩ, simultaneously. The gate voltage, used to control the direction of the switchable ferroelectric diode, was applied by using a source meter. A detailed schematic diagram of the α-In_2Se_3 device is displayed in Figure 5b. As shown in Figure 5c and 5d, the α-In_2Se_3 based ferroelectric rectifier can perform obvious rectifying properties. The obvious rectified output voltage signals could be observed when both the negative and positive gate biases are applied with an input sine waveform of V_{in} = ±2.5 V. In addition, the dynamic rectifying performance of the α-In_2Se_3 based switchable half-wave rectifier can work with a maximun frequency of about 50 Hz

(Figure S11, Supporting Information). These results indicate that this kind of ferroelectric diode can effectively work as a switchable half-wave rectifier.[32]

3. Conclusion

In summary, we have demonstrated a gate-controlled switchable ferroelectric diode by utilizing the intrinsic coupling of IP and OOP polarizations in 2D α-In_2Se_3. Compared with other ferroelectrics based switchable diodes that can only reverse their IP polarization by applying lateral high voltage pulse, this kind of 2D ferroelectrics, which possesses a polarization coupling between IP and OOP dipoles, can be used to realize three-dimensional architecture and modulation of the ferroelectric device. This makes them more promising in practical applications because of their higher integration level, convenient controlling mechanism, and compatibility with CMOS technology.

4. Experimental Section

Preparation of the α-In_2Se_3 nanoflakes: The α-In_2Se_3 nanoflakes were grown by using a chemical vapor deposition method. In brief, 0.1g Se (99.998%, Aladdin) was put into the upstream of quartz boats, and 0.05g In_2O_3 (99.99%, Aladdin) powders were put into the downstream. The fresh mica substrate, peeled off from a thick mica flake without other treatment, was put on the top of In_2O_3 powders as the substrate. The temperatures were set as 350 °C and 660 °C for Se and In_2O_3 powders, respectively. Argon gas was used as a carrier gas, and hydrogen gas served as the reductant, with a flow rate of 20 and 10 sccm, respectively. The pressure in the chamber was kept at an atmosphere for the whole reaction progress. After the reaction, the chamber was cooled down to room temperature very slowly (-1 °C/min) to guarantee the α-In_2Se_3 production. The α-In_2Se_3 nanoflakes grown on mica and bulk α-In_2Se_3 were taken out from the furnace in the end.

Characterizations: The Raman spectra of the sample were obtained by using a micro-Raman spectrometer system (HORIBA, HR800) and a 100× (0.9 NA) objective lens (Olympus, BX41). The excitement wavelength of the laser is 638 nm with a power of about 0.15 mW. The TEM and SEAD measurements were carried out on a TEM (JEM 2100F) instrument with an accelerating

voltage of 200 kV. The In_2Se_3 samples were transferred onto a TEM grid by using a polymethyl methacrylate (PMMA) assistant method for measurements.

The PFM measurements were carried out on a commercial instrument (Asylum Researcher, Cypher ES, USA) using contact mode, with a conductive Pt/Ir-coating cantilever (EFM, Nanoworld), and the resonant frequency and spring constant are 75 kHz and 2.8 N/m, respectively. The In_2Se_3 samples were transferred onto the Au/Si substrate for measurements. The statical domain structures were performed using the dual AC resonance tracking (DART) PFM with the amplitude of ac voltage V_{AC}=0.5 V, and the scanning rate is 1 Hz. The local piezoelectric response was measured using switch spectroscopy PFM (SSPFM), and the electrical signal applied on the probe is comprised of a constant ac voltage V_{AC}=0.5 V, and a triangle-square signal of a DC voltage to generate polarization switching. At this measurement, the vertical (VPFM) and lateral (LPFM) domain switching signals were investigated using the Vector PFM, and the scanning rate of writing and reading domain process both is 1 Hz and the AC voltage still is 0.5 V.

For SHG measurement, a femtosecond laser with an alpha 300RS+ Raman spectroscopy was used as the excitation source. The input laser was generated by a mode-locked Ti: sapphire with a pulse duration of 140 fs and a repetition rate of 80 MHz and filtered into optical parametric oscillator (Chameleon Compact OPOVis). The output laser beam was focused on the sample by 100× objective with a spot size of about 1.8 μm^2. SHG measurements were performed in a reflection geometry under normal incidence excitation. For the SHG polarization measurement, the collected SHG signal, which is parallel to input polarized light, was sent through a linear polarized analyzer by rotating the sample with a step of 10° relative to the fixed light polarization.

Fabrication of the α-In_2Se_3 devices: First, a triangular single crystal In_2Se_3 transferred onto SiO_2/Si (100 nm/500 μm) substrate with different contrast was selected using optical microscope (Olympus, BX41), and carbon fiber with a diameter of 7 μm was used as a shadow mask and put onto the top

of In_2Se_3 samples. The channel direction is perpendicular to [0120] axis, which can be defined through its triangular shape. Then, 50 nm Au as electrodes were deposited via thermal evaporation and the carbon fiber was removed after Au deposition.

Electrical measurements: Electrical characterizations of the device were performed by using a semiconductor characterization system (Keithley 4200-SCS) with a preamplifier (4225-RPM), and a probe station (Lakeshore). The measurements were carried out at ambient temperature and pressure. For the rectifier circuit measurement, an oscilloscope (Keysight, MSO-X 3104T) was used as the signal generator and the output signals detector. The gate voltage was applied by using a source meter (Keithley, 2400-SCS).

Supporting Information

Supporting Information is available from the Wiley Online Library or from the author.

Acknowledgments

M. Dai and K. Li contribut equally to this work. This work is supported by the National Natural Science Foundation of China (Nos. 61390502, 61505033 and 21825103), the Foundation for Innovative Research Groups of the National Natural Science Foundation of China (No. 51521003), the National Postdoctoral Science Foundation of China (Nos. 2017M621254, 2018T110280), the Heilongjiang Provincial Postdoctoral Science Foundation (LBH-TZ1708), the Self-Planned Task (SKLRS201607B) of State Key Laboratory of Robotics and System (HIT), and Key Laboratory of Micro-systems and Micro-structures Manufacturing of Ministry of Education, Harbin Institute of Technology (2017KM003).

Received: ((will be filled in by the editorial staff))

Revised: ((will be filled in by the editorial staff))

Published online: ((will be filled in by the editorial staff))

References

[1] J. F. Scott, *Science* **2007**, *315*, 954.
[2] M. M. Vopson, *Crit. Rev. Solid State Mater. Sci.* **2015**, *40*, 223.
[3] A. R. Damodaran, S. Pandya, J. C. Agar, Y. Cao, R. K. Vasudevan, R. J. Xu, S. Saremi, Q. Li, J. Kim, M. R. McCarter, L. R. Dedon, T. Angsten, N. Balke, S. Jesse, M. Asta, S. V. Kalinin, L. W. Martin, *Adv. Mater.* **2017**, *29*, 1702069.
[4] V. Garcia, M. Bibes, *Nat. Commun.* **2014**, *5*, 4289.
[5] Z. N. Xi, J. J. Ruan, C. Li, C. Y. Zheng, Z. Wen, J. Y. Dai, A. D. Li, D. Wu, *Nat. Commun.* **2017**, *8*, 15217.
[6] W. J. Xu, P. F. Li, Y. Y. Tang, W. X. Zhang, R. G. Xiong, X. M. Chen, *J. Am. Chem. Soc.* **2017**, *139*, 6369.
[7] M. M. Yang, M. Alexe, *Adv. Mater.* **2018**, *30*, 1704908.
[8] K. Chang, J. W. Liu, H. C. Lin, N. Wang, K. Zhao, A. M. Zhang, F. Jin, Y. Zhong, X. P. Hu, W. H. Duan, Q. M. Zhang, L. Fu, Q. K. Xue, X. Chen, S. H. Ji, *Science* **2016**, *353*, 274.
[9] A. Belianinov, Q. He, A. Dziaugys, P. Maksymovych, E. Eliseev, A. Borisevich, A. Morozovska, J. Banys, Y. Vysochanskii, S. V. Kalinin, *Nano Lett.* **2015**, *15*, 3808.
[10] F. C. Liu, L. You, K. L. Seyler, X. B. Li, P. Yu, J. H. Lin, X. W. Wang, J. D. Zhou, H. Wang, H. Y. He, S. T. Pantelides, W. Zhou, P. Sharma, X. D. Xu, P. M. Ajayan, J. L. Wang, Z. Liu, *Nat. Commun.* **2016**, *7*, 12357.
[11] Z. Liu, Y. H. Sun, D. J. Singh, L. J. Zhang, *Adv. Electron. Mater.* **2019**, *5*, 1900089.
[12] W. J. Ding, J. B. Zhu, Z. Wang, Y. F. Gao, D. Xiao, Y. Gu, Z. Y. Zhang, W. G. Zhu, *Nat. Commun.* **2017**, *8*, 14956.
[13] C. X. Zheng, L. Yu, L. Zhu, J. L. Collins, D. Kim, Y. D. Lou, C. Xu, M. Li, Z. Wei, Y. P. Zhang, M. T. Edmonds, S. Q. Li, J. Seidel, Y. Zhu, J. Z. Liu, W. X. Tang, M. S. Fuhrer, *Sci. Adv.* **2018**, *4*, eaar7720.
[14] Y. Zhou, D. Wu, Y. H. Zhu, Y. J. Cho, Q. He, X. Yang, K. Herrera, Z. D. Chu, Y. Han, M. C. Downer, H. L. Peng, K. J. Lai, *Nano Lett.* **2017**, *17*, 5508.
[15] C. J. Cui, W. J. Hu, X. G. Yan, C. Addiego, W. P. Gao, Y. Wang, Z. Wang, L. Z. Li, Y. C. Cheng, P. Li, X. X. Zhang, H. N. Alshareef, T. Wu, W. G. Zhu, X. Q. Pan, L. J. Li, *Nano Lett.* **2018**, *18*, 1253.
[16] S. M. Poh, S. J. R. Tan, H. Wang, P. Song, I. H. Abidi, X. Zhao, J. D. Dan, J. S. Chen, Z. T. Luo, S. J. Pennycook, A. H. C. Neto, K. P. Loh, *Nano Lett.* **2018**, *18*, 6340.
[17] J. Xiao, H. Y. Zhu, Y. Wang, W. Feng, Y. X. Hu, A. Dasgupta, Y. M. Han, Y. Wang, D. A. Muller, L. W. Martin, P. A. Hu, X. Zhang, *Phys. Rev. Lett.* **2018**, *120*, 227601.
[18] F. Xue, W. J. Hu, K. C. Lee, L. S. Lu, J. W. Zhang, H. L. Tang, A. Han, W. T. Hsu, S. B. Tu, W. H. Chang, C. H. Lien, J. H. He, Z. D. Zhang, L. J. Li, X. X. Zhang, *Adv. Funct. Mater.* **2018**, *28*, 1803738.
[19] C. J. Zhou, Y. Chai, *Adv. Electron. Mater.* **2017**, *3*, 1600400.
[20] X. Zhou, J. X. Cheng, Y. B. Zhou, T. Cao, H. Hong, Z. M. Liao, S. W. Wu, H. L. Peng, K. H. Liu, D. P. Yu, *J. Am. Chem. Soc.* **2015**, *137*, 7994.
[21] M. J. Dai, Z. G. Wang, F. K. Wang, Y. F. Qiu, J. Zhang, C. Y. Xu, T. Y. Zhai, W. W. Cao, Y. Q. Fu, D. C. Jia, Y. Zhou, P. A. Hu, *Nano Lett.* **2019**, *19*, 5410.
[22] T. Li, K. Y. Zeng, *Adv. Mater.* **2018**, *30*, 1803064.
[23] O. Kwon, D. Seol, D. Lee, H. Han, I. Lindfors-Vrejoiu, W. Lee, S. Jesse, H. N. Lee, S. V. Kalinin, M. Alexe, Y. Kim, *Adv. Mater.* **2018**, *30*, 1703675.
[24] P. Li, J. W. Zhai, B. Shen, S. J. Zhang, X. L. Li, F. Y. Zhu, X. M. Zhang, *Adv. Mater.* **2018**, *30*, 1705171.
[25] J. Luo, W. Sun, Z. Zhou, H. Y. Lee, K. Wang, F. Y. Zhu, Y. Bai, Z. J. Wang, J. F. Li, *Adv.*

Electron. Mater. **2017**, *3*, 1700226.

[26] H. Yan, Z. X. Feng, S. L. Shang, X. N. Wang, Z. X. Hu, J. H. Wang, Z. W. Zhu, H. Wang, Z. H. Chen, H. Hua, W. K. Lu, J. M. Wang, P. X. Qin, H. X. Guo, X. R. Zhou, Z. G. G. Leng, Z. K. Liu, C. B. Jiang, M. Coey, Z. Q. Liu, *Nat. Nanotechnol.* **2019**, *14*, 131.

[27] C. Wang, K. J. Jin, Z. T. Xu, L. Wang, C. Ge, H. B. Lu, H. Z. Guo, M. He, G. Z. Yang, *Appl. Phys. Lett.* **2011**, *98*, 192901.

[28] T. Choi, S. Lee, Y. J. Choi, V. Kiryukhin, S. W. Cheong, *Science* **2009**, *324*, 63.

[28] C. Ge, C. Wang, K. J. Jin, H. B. Lu, G. Z. Yang, *Nano-Micro Lett.* **2013**, *5*, 81.

[30] D. Lee, S. H. Baek, T. H. Kim, J. G. Yoon, C. M. Folkman, C. B. Eom, T. W. Noh, *Phys. Rev. B* **2011**, *84*, 125305.

[31] J. Zhou, P. Fei, Y. D. Gu, W. J. Mai, Y. F. Gao, R. Yang, G. Bao, Z. L. Wang, *Nano Lett.* **2008**, *8*, 3973.

[32] J. Y. Wu, Y. T. Chun, S. P. Li, T. Zhang, D. P. Chu, *ACS Appl. Mater. Interfaces* **2018**, *10*, 24613.